

Desiccation Patterns of Particle Laden Salt Droplets

Manikuntala Mukhopadhyay[†], Sri Ganesh Subramanian[†], Anashwara Nair[†], Debasish Sarkar[‡],

Sunando DasGupta[†]

[†]Department of Chemical Engineering, Indian Institute of Technology Kharagpur, West Bengal
- 721302, India.

[‡]Department of Chemical Engineering, Calcutta University, Kolkata, West Bengal - 700009,
India.

Corresponding author:

Email: sunando@che.iitkgp.ac.in

Ph.: +91 - 3222 - 283922

Abstract:

Drying of complex fluids leads to the formation of several intricate patterns where each component plays a unique role in determining the final dried morphologies. Salts form an essential component of body fluids (viz. blood, urine, saliva) and of buffer solutions, and hence, understanding the sole effect of salts on the dried patterns of the complex fluids has become imperative. In the present investigation, the exclusive effects of some commonly available salts on the final dried patterns of model solutions, in presence of polystyrene particles, have been explored. Fascinating results have been observed as the sole presence of salts were found to alter the final dried patterns of the particle suspensions. To delve deeper into the physics of the evaporation dynamics, a qualitative analysis has also been undertaken to estimate the predominant forces affecting the dried droplet morphologies. This investigation can serve as a baseline for understanding the underlying mechanisms involved during the drying of complex fluids to further aid in disease diagnosis.

1. Introduction:

Appearance of fascinating patterns after drying of colloidal droplets has gained significant interest in the field of interfacial science in the last few decades owing to its applications in healthcare and disease detection. Following the pioneering work of Deegan [1], several researchers have taken a keen interest in understanding the fundamentals of droplet evaporation of pure and complex fluids and the underlying mechanisms controlling the deposition patterns, to manipulate them for specific uses in varied fields like spray painting, inkjet printing, and surface patterning to name a few [2,3]. Through these investigations, it was observed that the final dried patterns depended on several factors such as the components of the droplets and their internal interactions, the nature of the substrate, its wettability, and rheology amongst others [4]. Apart from these, external parameters like temperature and relative humidity [2], also influence the rate of evaporation, giving rise to varied morphological patterns like the coffee ring [1], uniform deposition [5], multiple rings [6], fingering patterns [7], and crystal-like structures [8] to name a few. On the other hand, studies were also conducted to explore different methodologies to prevent the solute transportation to the contact line, as the coffee ring effect was found to reduce the performances of several commercial processes like printing, analysis of biochemical assays, patterning of structures etc. [9]. Instigating additional flow fields in the drying droplet such as Marangoni flows (by temperature or surface tension gradients), electroosmotic flows, electrowetting, vibrations and acoustic waves were found to reduce the extent of the outward driven capillary flow, thus averting the formation of coffee ring [9,10].

Gradually, as researchers started to explore the morphologies of the dried patterns of body fluids (viz. blood, plasma, urine etc.) for detection of diseases [11], it was understood that the final dried patterns of complex biofluids are more complex than that of pure solutions as even minor changes in the initial composition of the contents of the body fluids led to signatory differences in the final morphologies of the dried droplets. Thus, investigating the sole effect of various

components on the evaporation dynamics and the resulting drying patterns became essential for fundamental explorations and understanding, to further aid in disease detection [12–14]. Studies related to the drying of model systems/solutions became pre-eminent where these bio-fluids were modelled as a suspension of colloidal particles based on their size, shape, and concentrations. In some of the recent works, the effects of variation in the composition of proteins, colloidal particles, substrate temperatures and interplay of various predominant forces on the solutes during the drying of the sessile droplets has been considered to ascertain their effects on the final desiccation patterns [15–19].

Though ions form a very important component of the body fluids, most of these model solutions were prepared using deionized water. To discern the influence of basic components in a biofluid droplet on the final dried morphologies, proteins and salts were mixed in various concentrations [17], and it was concluded that the patterns could be manipulated by altering the initial ratios of the components in the solutions. Also, the effects of concentration and substrate nature on the morphological alterations of human erythrocytes were studied using blood samples diluted with phosphate buffer solutions [12]. The dried patterns of the diluted blood samples averted the formation of the ‘coffee ring’ and instead showed a central cluster pattern.

Owing to the significance of ions in complex fluids, studies investigating the hydrodynamics associated with the evaporation of sessile droplets of aqueous saline solutions have been conducted to understand the flow of ions and the subsequent formation of discrete salt crystals [20–23]. In an investigation relating to the effect of salt concentration on the forces acting on the particles near the contact line, it was observed that, during drying, the particles got adsorbed on the deposited salt which resulted in the reduced mobility of the particles [24]. From scrupulous literature review it becomes clear that although there exist a few studies which underscore the effect of particle shape [25,26], the influence of proteins and other biological entities [16,17,27] and the overall evaporation dynamics of aqueous saline solutions [20,21,23],

these studies have often failed to consider the sole underlying effect of salts on the final signatory dried patterns of complex fluids.

In the present work, the exclusive effects of some commonly available salts on the final dried patterns of model solutions have been explored. Aqueous suspensions of polystyrene particles (of varied sizes) were prepared in salt solutions to uncover the influence of multivalent ions on the final dried patterns. Six salts with multivalent co-ions viz. NaCl, Na₂HPO₄, NaH₂PO₄, Na₂SO₄, MgSO₄ and Na₃PO₄ have been chosen in the present case, based on their importance in many natural processes, occurrence in the body fluids and in the buffer solutions [17,23]. Polystyrene particles of four different sizes, were used to understand the influence of salts on the resultant drying patterns of colloids. Additionally, a qualitative analysis has also been undertaken to estimate the predominant forces affecting the final droplet morphologies to provide an initial conception of the sole effect of salts on the drying patterns to further facilitate in disease detection and other commercial purposes. The findings of this investigation could serve as a baseline for explicating the fundamental underlying physics of the mechanisms involved during the drying of complex fluids.

2. Materials and Methods:

2.1. Colloidal Suspension Preparation:

Six salts, namely Sodium chloride (NaCl), Sodium phosphate dibasic (Na₂HPO₄), Sodium phosphate monobasic (NaH₂PO₄), Sodium sulphate (Na₂SO₄), Magnesium sulphate (MgSO₄) and Trisodium phosphate (Na₃PO₄) have been used in the present study to uncover the sole effect of salts in the final dried patterns of the model solutions. All the salts were purchased from Sisco Research Laboratories Pvt. Ltd. (SRL), India. Each of these salts were dissolved in deionized water to prepare stock solutions of a fixed concentration (100mM). It must be highlighted that the concentration of the salt solutions was taken to be 100mM, owing to its biological equivalence to physiological conditions.

Colloidal suspensions of neutrally charged spherical polystyrene microparticles (purchased from Merck), of diameters 1 μm , 3 μm , 7 μm and 10 μm , were used to make the model solutions. The particles' density was around 1050 kg/m^3 according to the manufacturer's specifications sheet. Specific volumes of each of these microparticles were added to the salt solutions, to form the final suspension. The samples were prepared by varying the volumetric ratio of polystyrene based microparticles and 100 mM of salt solution in three different concentration ratios (v/v) of 1:30, 1:50 and 1:70. The control samples were prepared, in a similar manner, by adding precise volumes of polystyrene particles in deionized (DI) water in the three aforesaid concentrations (v/v). Once the final sample was prepared, all of them were sonicated for about 30 minutes, prior to experiment to ensure uniform suspension and to prevent particle aggregation. It must be noted that henceforth all concentrations that has been reported are volume fractions unless otherwise specified.

2.2. Substrate Preparation for Droplet Drying:

Indium Tin Oxide (ITO) coated glass slides (Material Composition: SiO_2 - 69%, In_2O_3 - 23%, SnO_2 - 8%), procured from Sigma Aldrich were used as substrates in the present study. They were subjected to a thorough cleaning protocol that comprised of ultrasonication with acetone, followed by de-ionized water (10 minutes each). The cleaned slides were dried in a hot air oven at 95°C to ensure complete removal of surface moisture. It must be noted that the roughness of glass slides is not consistent and varies with different batches and manufacturers. Hence, ITO coated glass slides have been used in the present investigation to maintain uniformity in the properties of the substrate as the main objective of the current work was to explore the effects of salts on the drying patterns, keeping every other variable constant.

2.3. Sample Characterization:

The pertinent physicochemical properties of the samples were evaluated. The first of these was the estimation of the contact angle and surface tension using a Goniometer (250 G1, Ram'ehart,

Germany), by placing sessile droplets (1 μL) of the samples on cleaned ITO coated glass slides. The initial contact angles and the surface tension for all the samples were found to be $76^{\circ}\pm 2^{\circ}$ and 71.55 ± 0.1 mN/m respectively. The zeta potentials (Malvern Instruments, Model: ZEN 3600) and pH of the samples were also evaluated (Labtronics, Model: LT-501) as reported in Table 3.1. The dielectric constants of the diluted salt solutions (used in the present study) were also measured (Keysight E4980A LCR meter) and were found to be 78 ± 0.8 .

Table 1: Characterization of samples

Solution	Zeta Potential (mV)	pH
NaCl	-2.4 ± 0.1	5.1 ± 0.1
Na_2HPO_4	-6.4 ± 0.5	8.6 ± 0.1
NaH_2PO_4	-3.9 ± 0.5	4.2 ± 0.1
Na_2SO_4	-9.3 ± 0.6	4.5 ± 0.1
MgSO_4	-2.6 ± 0.04	5.3 ± 0.1
Na_3PO_4	-12.9 ± 0.2	11 ± 0.1
DI water	-0.82 ± 0.06	5.2 ± 0.1

2.4. Experimental Procedure:

Sessile droplets of 1 μL volume were allowed to dry on cleaned ITO coated glass slides (for about 30 minutes to ensure complete drying). The final dried patterns were then observed using a $5\times$ objective lens under an optical microscope (LEICA DMi8 A) in the transmission mode. All the experiments were conducted at room temperature (27 ± 5 $^{\circ}\text{C}$) and humidity level 40-55% (measured using a hygrometer). The variations in the ambient conditions did not significantly affect the formation of the final dried patterns, as the results were found to be accurate, consistent, and repeatable. Figure 3.1 represents the schematic of the experimental set up.

As the wetted diameter of the deposited droplet (2.1 mm) was below the capillary length (2.7 mm) throughout the entire study, the shape of the droplets was, thus, approximated as spherical cap. It must be noted that the entire set of experiments were repeated at least 10 times to ensure reproducibility and repeatability.

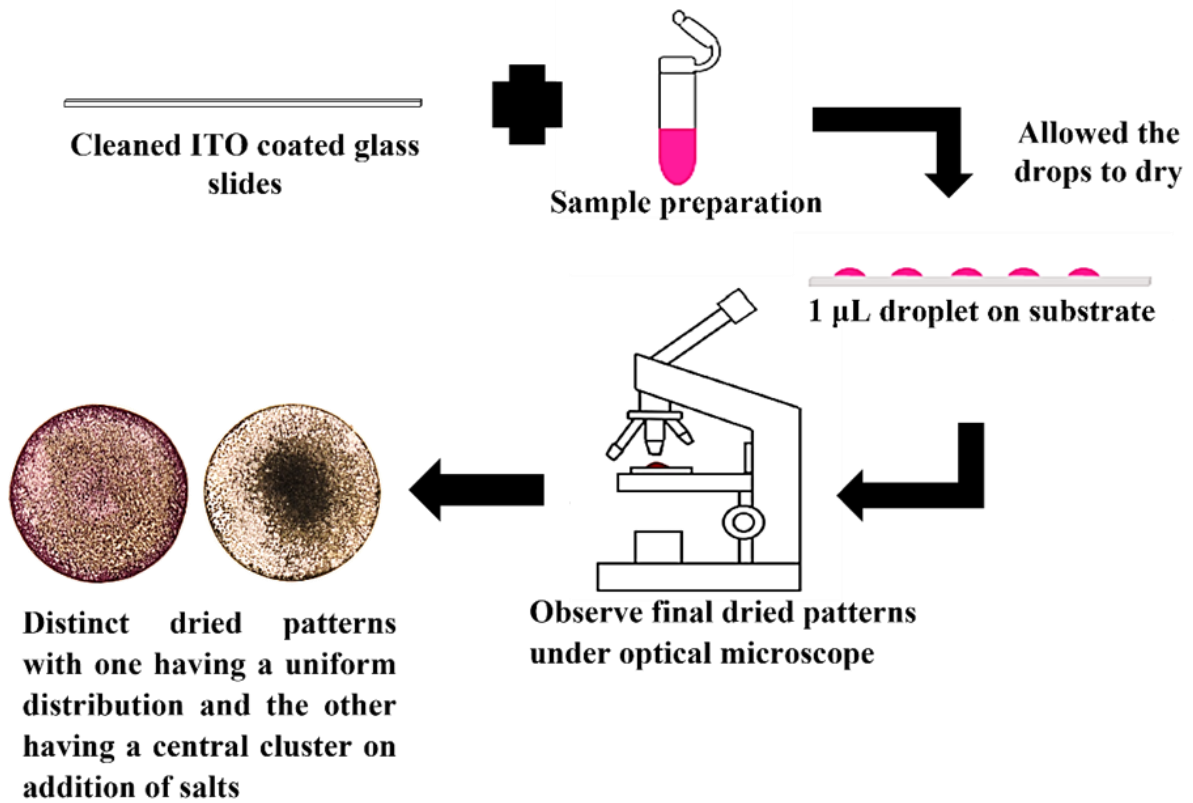


Figure 1: Schematic of the experimental process

3. Theoretical Framework:

It is well known that in an evaporating droplet containing colloidal particles, the particles at the contact line experience various forces [28,29], as depicted in Figure 2. It needs to be mentioned as the temperature gradient across the evaporating droplet was very small [30], the droplet has been assumed to have a spatially uniform temperature. Thus, the temperature induced Marangoni flow has been safely neglected.

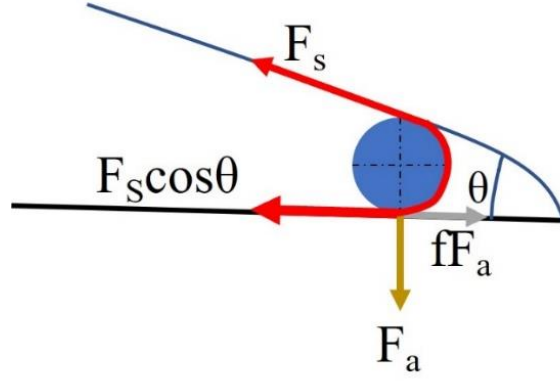


Figure 2: Schematic of the forces acting on a particle during evaporation.

In the early stages of droplet evaporation, due to the enhanced evaporation rate at the edges, the particles suspended in the droplet are carried radially outwards towards the contact line by the drag force (F_d) [28] represented by

$$F_d = 3\pi d_p \mu v_{rad} \alpha \quad (1)$$

where, d_p = diameter of the microparticles, μ is the dynamic viscosity of fluid, v_{rad} is the velocity of the evaporation driven flow and α is the drag coefficient.

Additionally, the suspended particles inside the droplet are also subjected to short range forces, van der Waals and electrostatic interactions, which together constitute the DLVO forces [31]. In this investigation, the focus is on the domain of large Peclet numbers, thus, the non-DLVO forces acting on the particles along with the other random forces causing Brownian motion are not considered.

The attractive van der Waals interaction forces between two particles in a fluid medium can be evaluated as [31]

$$F_{vdw-pp} = -\frac{A}{6D^2} \left(\frac{r_1 r_2}{r_1 + r_2} \right) \quad (2)$$

where A is the Hamaker constant between the particles in a fluid medium, D is the minimum separation distance, r_1 and r_2 are the radii of the particles. For cases where $r_1 = r_2 = r$, equation (3.2) becomes

$$F_{vdw-pp} = -\frac{Ar}{12D^2} \quad (3)$$

Similarly, the van der Waals force between the particles and the substrate can be evaluated as [31]

$$F_{vdw-ps} = -\frac{2A'r^3}{3D^2(D+2r)^2} \quad (4)$$

Where A' is the Hamaker constant between the particles and the substrate in the fluid medium.

Next, the electrostatic interactions between the two particles in the fluid medium can be expressed as [31]

$$F_{el-pp} = \kappa Z e^{-\kappa D} \left(\frac{r_1 r_2}{r_1 + r_2} \right) \quad (5)$$

where $Z = 64\pi\epsilon_0\epsilon \left(\frac{k_B T}{e} \right)^2 \gamma_1$ and $\gamma_1 = \tanh^2 \left(\frac{ze\psi_0}{4k_B T} \right)$

and the Debye length $\kappa^{-1} = \left(\frac{\epsilon_0 \epsilon k_B T}{\sum_i \rho_\infty e^2 z_i^2} \right)^{1/2}$

where ϵ_0 is permittivity of free space, ϵ is the dielectric constant, k_B is the Boltzmann constant, T is the absolute temperature, e is the elementary electron charge, ρ_∞ is the concentration of ions in the bulk and ψ_0 is the zeta potential of the solution.

Similarly for particle-substrate, the electrostatic interactions can be expressed as

$$F_{el-ps} = \kappa Z r e^{-\kappa D} \quad (6)$$

$$\text{and } Z = 64\pi\epsilon_0\epsilon \left(\frac{k_B T}{e}\right)^2 \gamma_1 \gamma_s, \quad \gamma_1 = \tanh\left(\frac{ze\psi_0}{4k_B T}\right), \quad \gamma_s = \tanh\left(\frac{ze\psi_s}{4k_B T}\right)$$

where ψ_s is the zeta potential of the substrate.

Thus, the total force acting on the particles in the vertically downward direction (represented by F_a in the Figure 3.2) due to the adhesion forces can be estimated as [29,32-34]

$$F_a = n(F_{vdw-ps} + F_{el-ps}) \quad (7)$$

where n denotes the total number of rows of particles that are present at the edge of the droplet [29,32]. For systems where the evaporation proceeds with the pinning of the contact line, a capillary meniscus is formed, once the height of the droplet reduces below the size of the particles that are present in it. Thus, along with the aforementioned forces, the suspended particles will also experience an inward pull (away from the contact line), known as the capillary/surface tension driven force, which can be expressed as [28,29,32]

$$F_s \cos \theta = 2\pi r \gamma \cos \theta \quad (8)$$

where γ is the surface tension of the liquid.

The subsequent motion of the particles would, thus, be a competition between the surface tension forces (represented by equation 8) and the frictional forces, fF_a (induced by the forces acting vertically downwards), where f is the frictional co-efficient (as depicted in Figure 2). It must be noted that equation 7 has been multiplied by n to account for all rows of particles that are present at the contact line, that would resist the inward capillary motion.

4. Results and Discussion:

4.1. Evaporation Modes:

For all the cases in the current investigation, the evaporation of the droplets proceeded in a constant contact radius (CCR) mode with the pinning of the contact line, as shown in Figures 3 and 4.

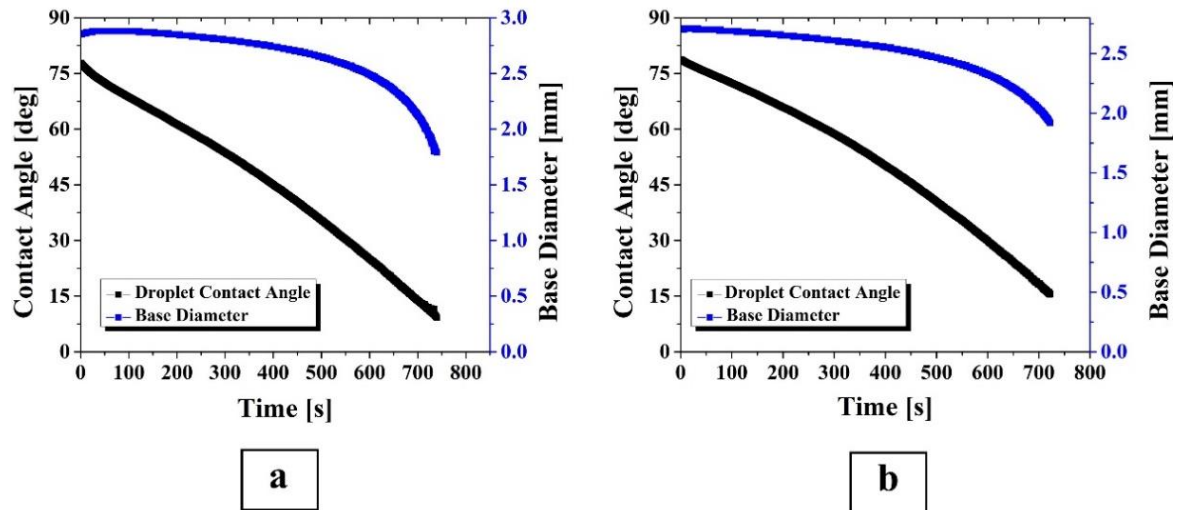


Figure 3: Representative graphs depicting variation of the contact angle and base diameter of the droplets with time. (a) Polystyrene particles of size - 1 μm (diameter) in 100 mM of NaH_2PO_4 solution at a concentration of 1:30 (v/v) (b) Polystyrene particles of size - 3 μm (diameter) in 100 mM of NaH_2PO_4 solution at a concentration of 1:30 (v/v)

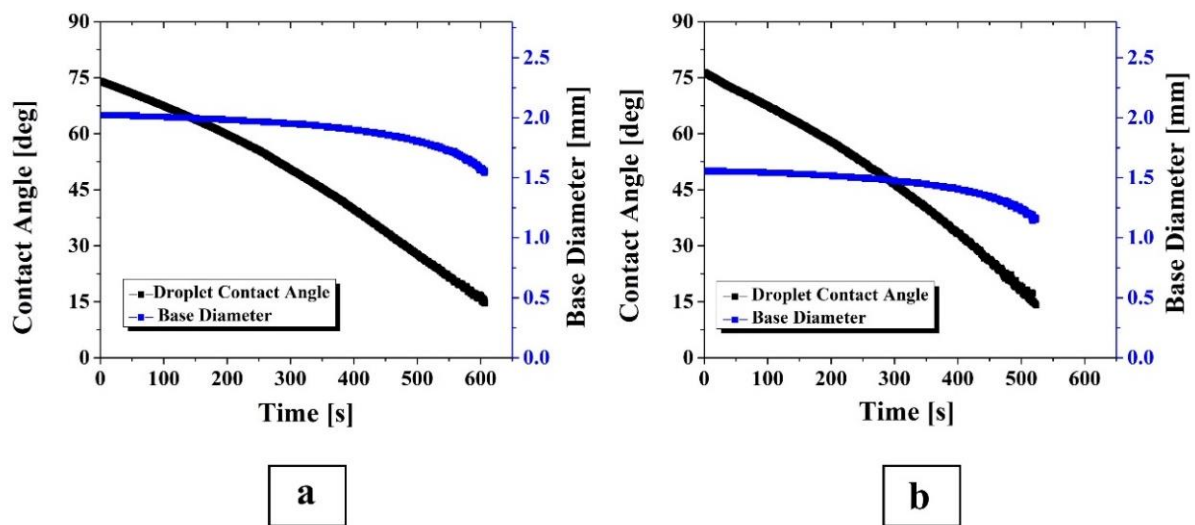


Figure 4: Representative graphs depicting variation of the contact angle and base diameter of the droplets with time. (a) Polystyrene particles of size - 7 μm (diameter) in 100 mM of NaH_2PO_4 solution at a concentration of 1:30 (v/v) (b) Polystyrene particles of size - 10 μm (diameter) in 100 mM of NaH_2PO_4 solution at a concentration of 1:30 (v/v)

As the surface here is hydrophilic, the liquid vapour meniscus has been considered to form a wedge with gradual reduction of the thickness from the apex towards the edge of the droplet [29,32-35]. The evaporation flux is highest at the edge of the droplet, thus the fluid along with the particles flow radially outwards to recuperate the greater loss of liquid.

4.2. Dried Deposition Patterns of Particles in Salt Solutions:

4.2.1. For Particle Sizes of 1 and 3 microns:

As stated in the previous section, the droplets of all the samples were allowed to dry naturally on cleaned ITO coated glass slides. The drying patterns of the samples prepared in salt solutions showed noticeable differences to the ones prepared in DI water. The results observed were fascinating as the sole presence of salts were found to suppress the coffee ring effect. A clear transition from the well-known coffee ring pattern to the uniform distribution pattern was observed (as depicted in Figures 5 through 7), and this transition was found to be consistent with all the salt solutions and concentrations.

It must be noted that, as reported in the literature, in absence of salt the thickness of the coffee ring increased with increasing particle concentration, as depicted in Figure 5 [35]

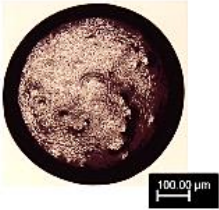
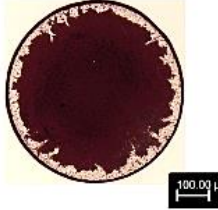
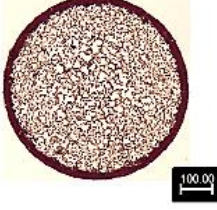
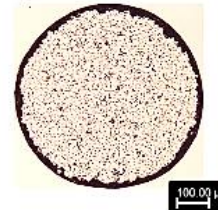
Particle Size	Concentration Ratio		
	1:30	1:50	1:70
1 micron			
3 micron			

Figure 5: Representative images showing the formation of coffee-ring in solutions comprising of particles (1 and 3 micron respectively) in DI water (the scale bar in the images represents a length of 100 μm)

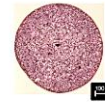
Salt Solution	Concentration Ratio			Salt Solution	Concentration Ratio		
	1:30	1:50	1:70		1:30	1:50	1:70
NaCl				Na ₂ SO ₄			
Na ₂ HPO ₄				MgSO ₄			
NaH ₂ PO ₄				Na ₃ PO ₄			
a				b			

Figure 6: Representative images showing the uniform distribution pattern in solutions comprising of particles of size 1 μm (diameter) and multivalent co-ions (the scale bar in the images represents a length of 100 μm)

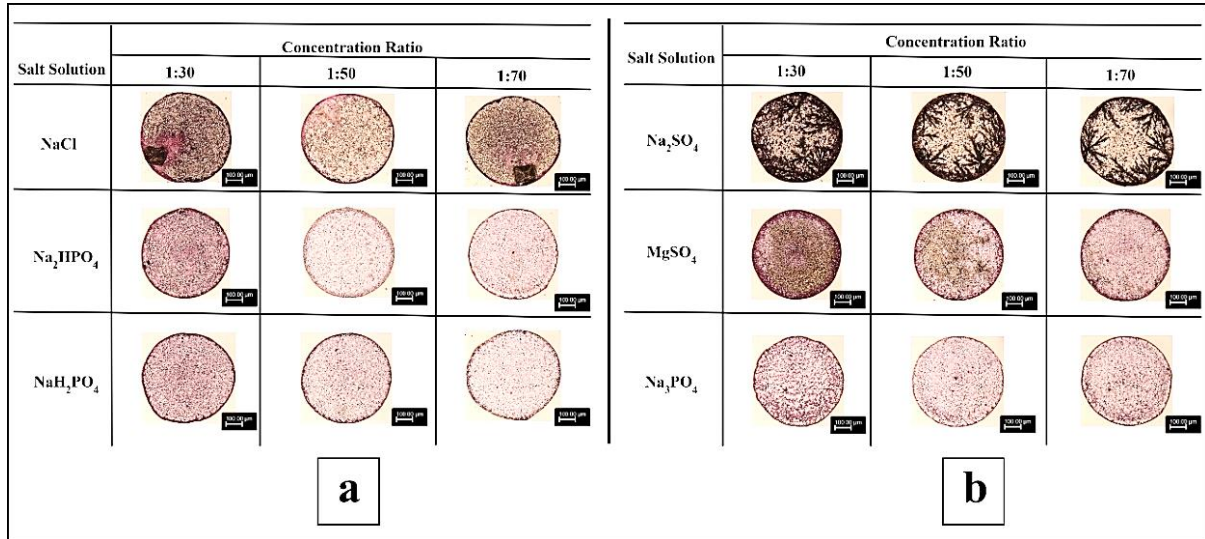


Figure 7: Representative images showing the uniform distribution pattern in solutions comprising of particles of size 3 μm (diameter) and multivalent co-ions (the scale bar in the images represents a length of 100 μm)

To delve deeper into the physics of the evaporation dynamics, a qualitative analysis has been undertaken to estimate the predominant forces affecting the final dried droplet morphologies.

To begin with, the settling velocities of the particles (V_s) have been estimated according to the

Stokes law, given by, $V_s = \frac{d_p^2(\rho_p - \rho)g}{18\mu}$, where d_p is the diameter of the particle, ρ_p is the

particle density, ρ is the density of water, g is the gravitational acceleration and μ is dynamic

viscosity of water. V_s of particles of sizes 1 and 3 microns are found to be in the order of ~ 3.02

$\times 10^{-8}$ and $\sim 2.72 \times 10^{-7}$ m/s respectively. Next, the velocity of the evaporation driven flow

(advection velocity) has been approximated as $V_e = \frac{j_{\max}}{\rho}$, where j_{\max} is the maximum

evaporation flux at the edge of the droplet and has been estimated by solving the analytical

expression as suggested by Hu and Larson [36]. For the present investigation, V_e is found to be in the order of $\sim 2 \times 10^{-7}$ m/s. As the settling velocities are either less than or in the same order of magnitude as the advection velocity, the outward flow will be predominant, thus, carrying the particles to the edge and leading to the formation of the coffee ring [35] (as depicted in Figure 5).

During the initial stages of drying, the capillary flows play a significant role in carrying the particles towards the edge ($F_d \sim 10^{-15}$ N, as detailed in Table 3) before the other interaction forces comes into effect [29]. As mentioned previously, the evaporation of the droplet, in the present case, proceeds with the pinning of the contact line with a gradual decrease in the height of the droplet. Once the height of the droplet reduces below the size of the particles, it leads to the formation of a capillary meniscus [28,32,33]. Subsequently the particles are subjected to an inward force, that is driven by surface tension, $F_s \cos \theta \sim 10^{-8}$ N. The subsequent motion of particles would then be a competition between the surface tension forces and the frictional forces, fF_a (that depends upon the van der Waals and the electrostatic interactions between the particles and the substrate, as represented by equation 7 and Figure 2). During the course of evaporation, as more particles start depositing at the edge, the adhesion forces amplify (with increase of n as shown in equation 7), further enhancing the frictional force. This finally counterbalances the surface tension driven force and leads to more deposition of particles at the contact line [28,29,32].

For samples where salts have been added, a subsequent change in the direction of flows was observed, that led to suppression of the coffee ring structure (as depicted in Figures 6 and 7). When a droplet containing particles and salt, begins to evaporate, the ions being smaller in size (in the range of picometres), move radially outwards towards the edge, faster than the particles, to replenish the enhanced loss of liquid at the edge of the droplet. With evaporation, as the size of the meniscus keeps reducing gradually, the ions and the particles both start moving towards the contact line and stops at the position where the thickness of the local meniscus matches their

respective heights [29,33,34]. Hence, the ions move closer to the contact line as compared to the particles. With the deposition of ions, their concentration at the edge will be significantly more than the apex of the droplet. Thus, this surface tension gradient will give rise to a Marangoni flow directed from the center of the droplet towards the contact line [20-22]. The liquid that will be carried by this Marangoni flow will be more than the evaporative losses, and as per the mass conservation, a flow will be induced at the base (at the liquid substrate interface) to carry the liquid back from the edge of the droplet [21]. It is this inward flow that will carry the particles along with the liquid from the periphery towards the center of the droplet.

In a recent study, it was observed that during the drying of a droplet, in presence of salts (>50mM), the particles showed some initial motion during the start of evaporation, but gradually their velocities dropped significantly due to adsorption [24], whereas in salt free droplets the particles showed frictionless motions. Thus, it can be hypothesized, in the present case, that while the fluid along with the particles were being carried back by the inward base flow from the edge towards the center of the droplet, they were adsorbed on the substrate, thus finally leading to the formation of the uniform distribution pattern. This hypothesis can be validated by the photomicrographs as obtained from the scanning electron microscope (FESEM-Jeol (Japan), JSM-7610F) (as depicted in Figures 8 and 9). The absence of salts clearly showed the formation of coffee ring structure, whereas, when the same sample was prepared in a salt solution, a clear adsorption of the particles on the substrate could be seen, thus finally giving rise to the uniform distribution pattern.

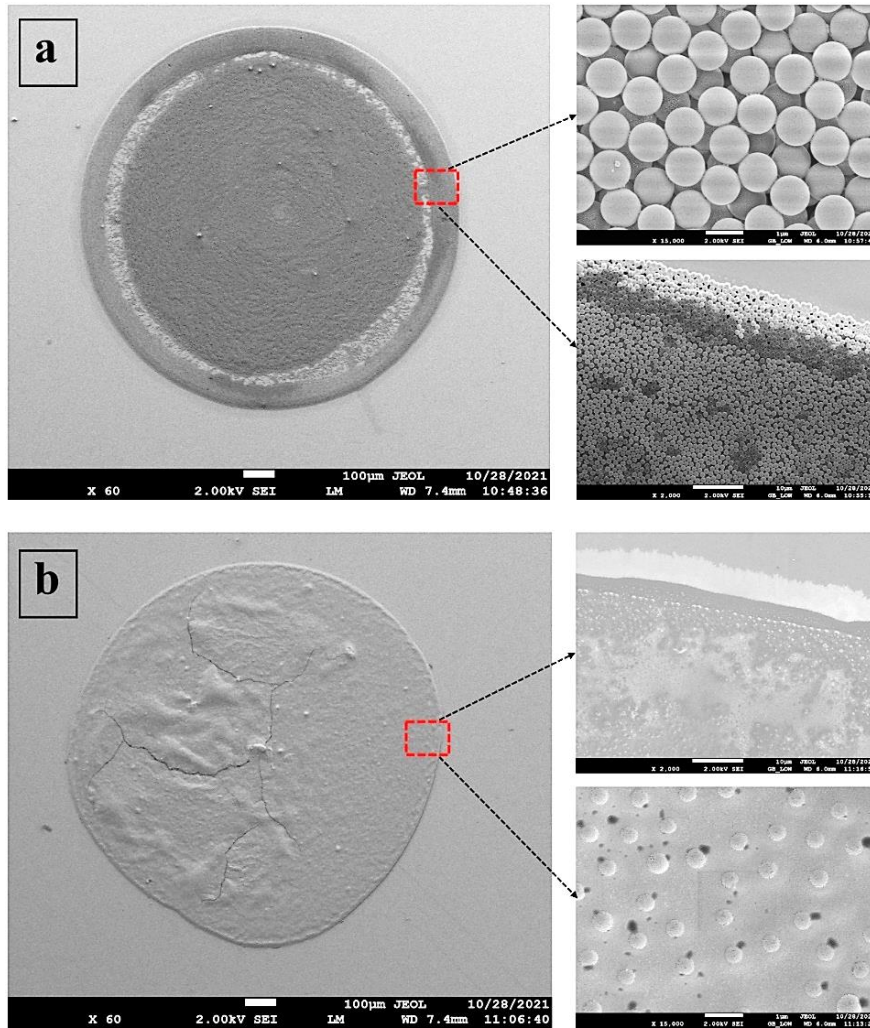


Figure 8: Scanning Electron Microscopy images of dried droplet patterns of 1-micron sized particles (a) In DI water (b) In presence of salt.

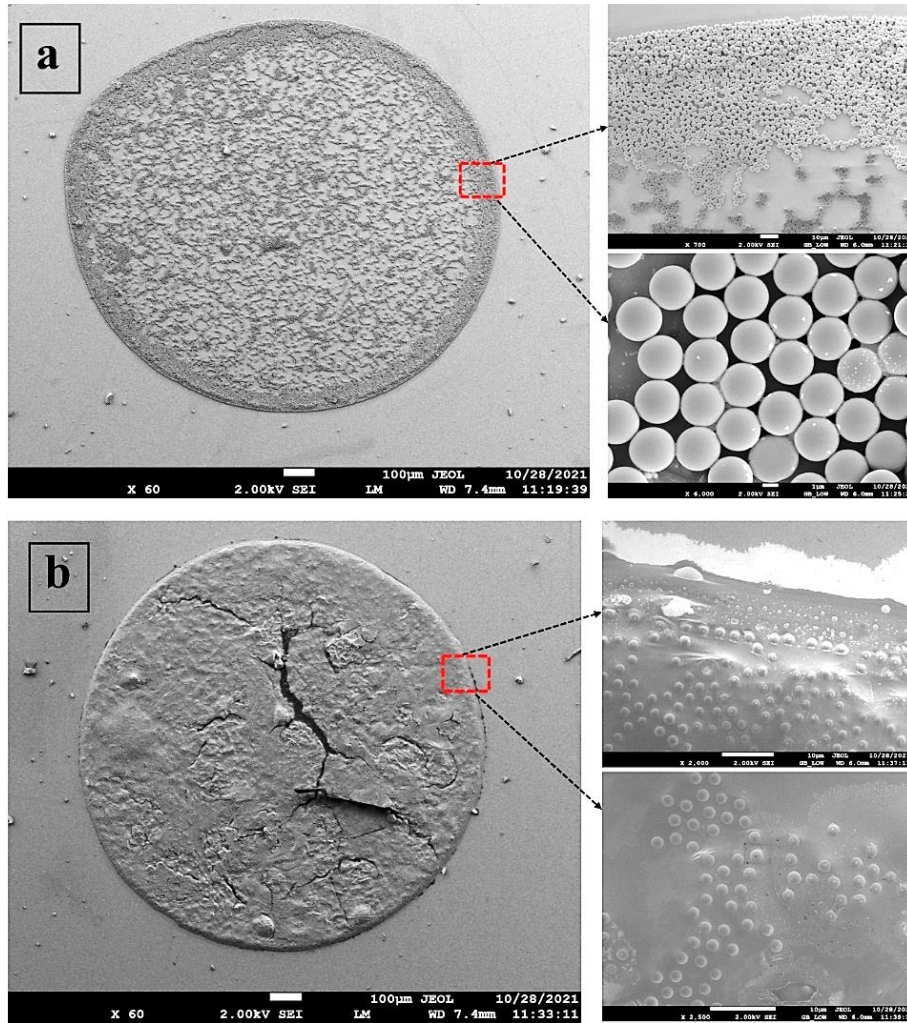


Figure 9: Scanning Electron Microscopy images of dried droplet patterns of 3-micron sized particles (a) In DI water (b) In presence of salt.

It must also be mentioned that, in presence of salt, as smaller number of particles are carried towards the edge of the droplet, the total frictional forces will be lesser than that of samples in absence of salt (as per equation 7). Thus, the frictional forces will not be able to overpower the inward forces, leading to the flow of the fluid along with the particles towards the center. The order of magnitude of all the relevant forces have been presented in Tables 3 and 4. It must be mentioned that the negative sign here denotes attractive force, and the positive sign denotes repulsive force. All the relevant parameters that have been used for the estimation of forces has been mentioned in Table 2.

Table 2: Details of parameters used for estimation of the predominant forces.

Physical Parameter	Value
Diameter of the microparticles, d_p	1 μm , 3 μm , 7 μm , 10 μm
Dynamic viscosity of fluid, μ	0.0009 Pa. s
Velocity of the evaporation driven flow, v_{rad}	2×10^{-7} m/s
Drag coefficient, α	1.9 [32]
Hamaker constant between the particles in a fluid medium, A	$\sim 0.4 \times 10^{-20}$ J [31]
Hamaker constant between the particles and the substrate in the fluid medium, A'	$\sim 0.4 \times 10^{-20}$ J [31]
Minimum separation distance, D	0.4 nm [32,37,38]
Debye length, κ^{-1}	<p>NaCl = 9.61×10^{-10} m</p> <p>Na_2HPO_4 = 5.56×10^{-10} m</p> <p>NaH_2PO_4 = 9.61×10^{-10} m</p> <p>Na_2SO_4 = 5.56×10^{-10} m</p> <p>MgSO_4 = 4.81×10^{-10} m</p> <p>Na_3PO_4 = 4.30×10^{-10} m</p> <p>DI water = 4.30×10^{-7} m</p>
Permittivity of free space, ϵ_0	8.85×10^{-10} F m ⁻¹
Dielectric constant, ϵ	78.4
Absolute temperature, T	298 K
Zeta potential of the solution, ψ_0	Mentioned in Table 3.1
Zeta potential of the substrate, ψ_s	- 39 mV

Table 3: Orders of magnitude of the forces acting on particles of size 1 μm in a drying droplet.

Solution	Surface Tension, $F_s \cos \theta$ (N)	Drag Force, F_d (N)	van der Waals, F_{vdw-pp} (N)	Electrostatic Interaction, F_{el-pp} (N)	van der Waals, F_{vdw-ps} (N)	Electrostatic Interaction, F_{el-ps} (N)
NaCl	5.47×10^{-8}	3.22×10^{-15}	-1.04×10^{-9}	8.59×10^{-12}	-2.08×10^{-9}	2.66×10^{-10}
Na₂HPO₄	5.47×10^{-8}	3.22×10^{-15}	-1.04×10^{-9}	7.78×10^{-11}	-2.08×10^{-9}	9.06×10^{-10}
NaH₂PO₄	5.47×10^{-8}	3.22×10^{-15}	-1.04×10^{-9}	2.27×10^{-11}	-2.08×10^{-9}	4.33×10^{-10}
Na₂SO₄	5.47×10^{-8}	3.22×10^{-15}	-1.04×10^{-9}	1.60×10^{-10}	-2.08×10^{-9}	1.30×10^{-9}
MgSO₄	5.47×10^{-8}	3.22×10^{-15}	-1.04×10^{-9}	1.33×10^{-11}	-2.08×10^{-9}	3.81×10^{-10}
Na₃PO₄	5.47×10^{-8}	3.22×10^{-15}	-1.04×10^{-9}	3.28×10^{-10}	-2.08×10^{-9}	1.90×10^{-9}
DI water	5.47×10^{-8}	3.22×10^{-15}	-1.04×10^{-9}	3.23×10^{-15}	-2.08×10^{-9}	3.01×10^{-13}

Table 4: Orders of magnitude of the forces acting on particles of size 3 μm in a drying droplet.

Solution	Surface Tension, $F_s \cos \theta$ (N)	Drag Force, F_d (N)	van der Waals, F_{vdw-pp} (N)	Electrostatic Interaction, F_{el-pp} (N)	van der Waals, F_{vdw-ps} (N)	Electrostatic Interaction, F_{el-ps} (N)
NaCl	1.64×10^{-7}	9.66×10^{-15}	-3.12×10^{-9}	2.58×10^{-11}	-6.25×10^{-9}	7.99×10^{-10}
Na₂HPO₄	1.64×10^{-7}	9.66×10^{-15}	-3.12×10^{-9}	2.33×10^{-10}	-6.25×10^{-9}	2.72×10^{-9}
NaH₂PO₄	1.64×10^{-7}	9.66×10^{-15}	-3.12×10^{-9}	6.80×10^{-11}	-6.25×10^{-9}	1.30×10^{-9}
Na₂SO₄	1.64×10^{-7}	9.66×10^{-15}	-3.12×10^{-9}	4.81×10^{-10}	-6.25×10^{-9}	3.90×10^{-9}
MgSO₄	1.64×10^{-7}	9.66×10^{-15}	-3.12×10^{-9}	3.99×10^{-11}	-6.25×10^{-9}	1.14×10^{-9}
Na₃PO₄	1.64×10^{-7}	9.66×10^{-15}	-3.12×10^{-9}	9.85×10^{-10}	-6.25×10^{-9}	5.71×10^{-9}

DI water	1.64×10^{-7}	9.66×10^{-15}	-3.12×10^{-9}	9.69×10^{-15}	-6.25×10^{-9}	9.02×10^{-13}
-----------------	-----------------------	------------------------	------------------------	------------------------	------------------------	------------------------

4.2.2. For Particle Sizes of 7 and 10 microns:

When the droplets containing bigger sized polystyrene particles were allowed to dry on the cleaned ITO coated glass slides, the presence or absence of salts were found to significantly influence the final dried patterns when compared to the samples prepared in DI water. The samples that were prepared in DI water left a uniform distribution pattern (as depicted in Figure 10), whereas the presence of salts led to formation of a central cluster (as shown in Figures 11 and 12).

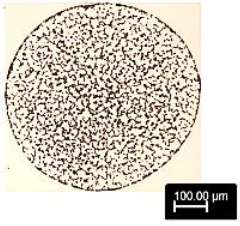
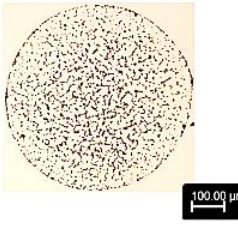
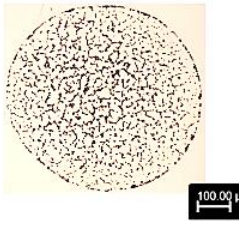
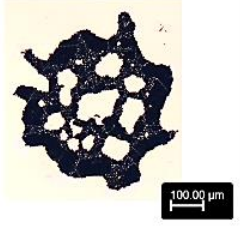
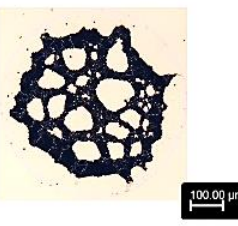
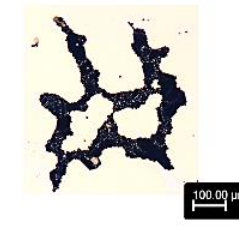
Particle Size	Concentration Ratio		
	1:30	1:50	1:70
7 micron			
10 micron			

Figure 10: Representative images showing the final dried patterns of solutions comprising of particles (7 and 10 micron respectively) in DI water (the scale bar in the images represents a length of 100 µm)

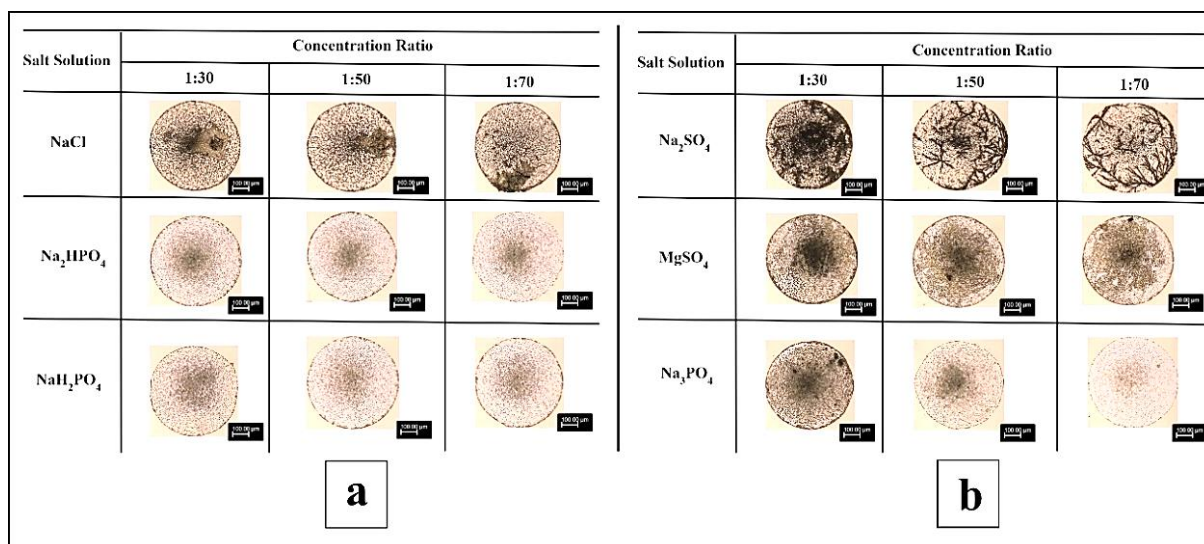


Figure 11: Representative images showing the central cluster pattern in solutions comprising of particles of size 7 μm (diameter) and multivalent co-ions (the scale bar in the images represents a length of 100 μm)

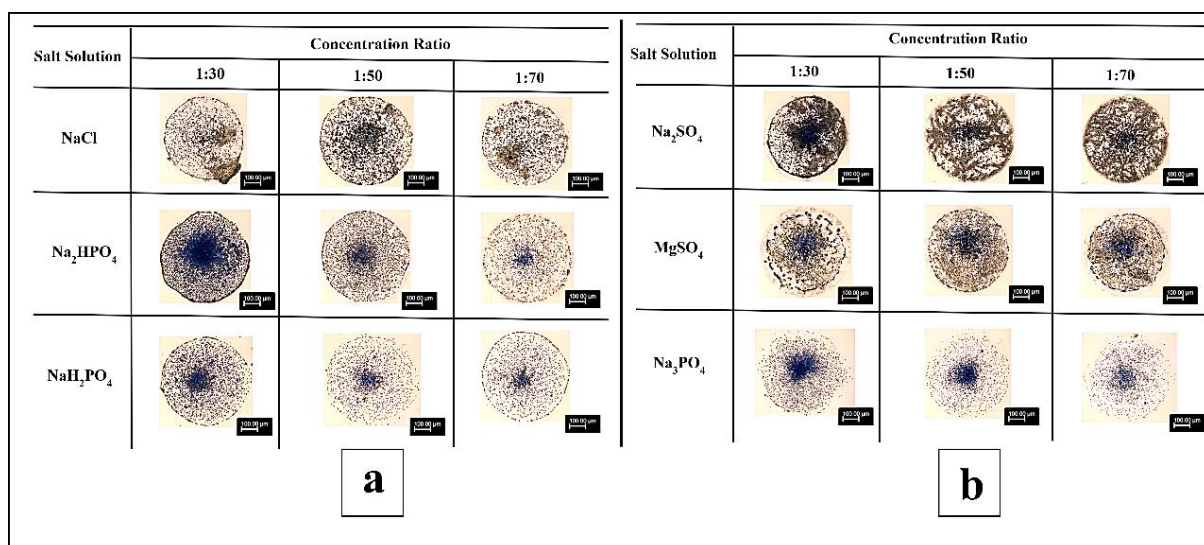


Figure 12: Representative images showing the central cluster pattern in solutions comprising of particles of size 10 μm (diameter) and multivalent co-ions (the scale bar in the images represents a length of 100 μm)

As already established in the literature [32,35,39], bigger particles tend to move inwards, due to greater capillary force acting on them, and finally result in the suppression of coffee ring. This is in line with the current observations when the suspensions were prepared using DI water. It must

be highlighted, that as the volumetric concentration of particles have been kept same in all the cases, the concentration of bigger particles was, hence, lesser than the smaller ones. Thus, with increase in size, fewer particles were available to pin the contact line. Moreover, the settling velocities of particles of sizes 7 and 10 μm were found to be in the order of 1.48×10^{-6} m/s and 3.02×10^{-6} m/s, which is one order of magnitude higher than the advection velocity ($\sim 2 \times 10^{-7}$ m/s). Thus, the larger sized microparticles had a greater tendency to settle down at a distance away from the contact line [35]. Also, due to the higher particle-particle attraction, they tended to adhere to one another while settling, thus suppressing the coffee ring formation [5]. The order of magnitude of the forces acting on the particles of sizes 7 μm and 10 μm have been depicted in Tables 5 and 6.

Table 5: Orders of magnitude of the forces acting on particles of size 7 μm in a drying droplet.

Solution	Surface Tension, $F_s \cos \theta$ (N)	Drag Force, F_d (N)	van der Waals, F_{vdw-pp} (N)	Electrostatic Interaction, F_{el-pp} (N)	van der Waals, F_{vdw-ps} (N)	Electrostatic Interaction, F_{el-ps} (N)
NaCl	3.83×10^{-7}	2.26×10^{-14}	-7.29×10^{-9}	6.01×10^{-11}	-1.46×10^{-8}	9.33×10^{-10}
Na₂HPO₄	3.83×10^{-7}	2.26×10^{-14}	-7.29×10^{-9}	5.44×10^{-10}	-1.46×10^{-8}	3.17×10^{-9}
NaH₂PO₄	3.83×10^{-7}	2.26×10^{-14}	-7.29×10^{-9}	1.59×10^{-10}	-1.46×10^{-8}	1.52×10^{-9}
Na₂SO₄	3.83×10^{-7}	2.26×10^{-14}	-7.29×10^{-9}	1.12×10^{-9}	-1.46×10^{-8}	4.55×10^{-9}
MgSO₄	3.83×10^{-7}	2.26×10^{-14}	-7.29×10^{-9}	9.30×10^{-11}	-1.46×10^{-8}	1.33×10^{-9}
Na₃PO₄	3.83×10^{-7}	2.26×10^{-14}	-7.29×10^{-9}	2.30×10^{-9}	-1.46×10^{-8}	6.67×10^{-9}
DI water	3.83×10^{-7}	2.26×10^{-14}	-7.29×10^{-9}	2.26×10^{-14}	-1.46×10^{-8}	1.05×10^{-12}

Table 6: Orders of magnitude of the forces acting on particles of size 10 μm in a drying droplet.

Solution	Surface Tension, $F_s \cos \theta$ (N)	Drag Force, F_d (N)	van der Waals, F_{vdw-pp} (N)	Electrostatic Interaction, F_{el-pp} (N)	van der Waals, F_{vdw-ps} (N)	Electrostatic Interaction, F_{el-ps} (N)
NaCl	5.47×10^{-7}	3.22×10^{-14}	-1.04×10^{-8}	8.59×10^{-11}	-2.08×10^{-8}	2.66×10^{-9}
Na₂HPO₄	5.47×10^{-7}	3.22×10^{-14}	-1.04×10^{-8}	7.78×10^{-10}	-2.08×10^{-8}	9.06×10^{-9}
NaH₂PO₄	5.47×10^{-7}	3.22×10^{-14}	-1.04×10^{-8}	2.26×10^{-10}	-2.08×10^{-8}	4.33×10^{-9}
Na₂SO₄	5.47×10^{-7}	3.22×10^{-14}	-1.04×10^{-8}	1.60×10^{-9}	-2.08×10^{-8}	1.30×10^{-8}
MgSO₄	5.47×10^{-7}	3.22×10^{-14}	-1.04×10^{-8}	1.33×10^{-10}	-2.08×10^{-8}	3.81×10^{-9}
Na₃PO₄	5.47×10^{-7}	3.22×10^{-14}	-1.04×10^{-8}	3.28×10^{-9}	-2.08×10^{-8}	1.90×10^{-8}
DI water	5.47×10^{-7}	3.22×10^{-14}	-1.04×10^{-8}	3.23×10^{-14}	-2.08×10^{-8}	3.01×10^{-12}

As mentioned previously, in presence of salts, the ions will deposit at the edges, thus inducing an inward base flow. This will further push the fluid along with the particles towards the center. The particles which were already slowed (because of their greater settling velocities) would thus finally settle at or near the center of the droplet, with very few particles reaching up to the contact line. The photomicrographs as obtained from the scanning electron microscope clearly show the differences in the final dried patterns in presence and absence of salts (as depicted in Figures 13 and 14).

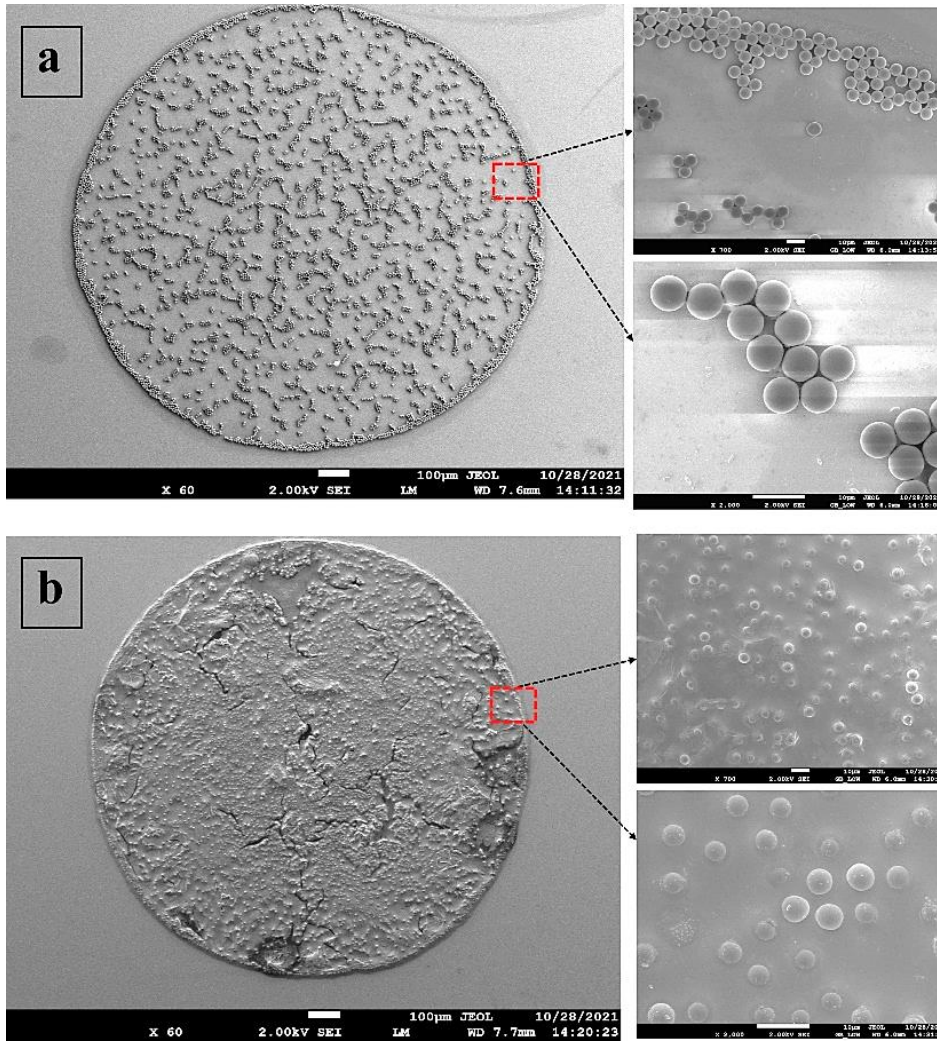


Figure 13: Scanning Electron Microscopy images of dried droplet patterns of 7-micron sized particles (a) In DI water (b) In presence of salt.

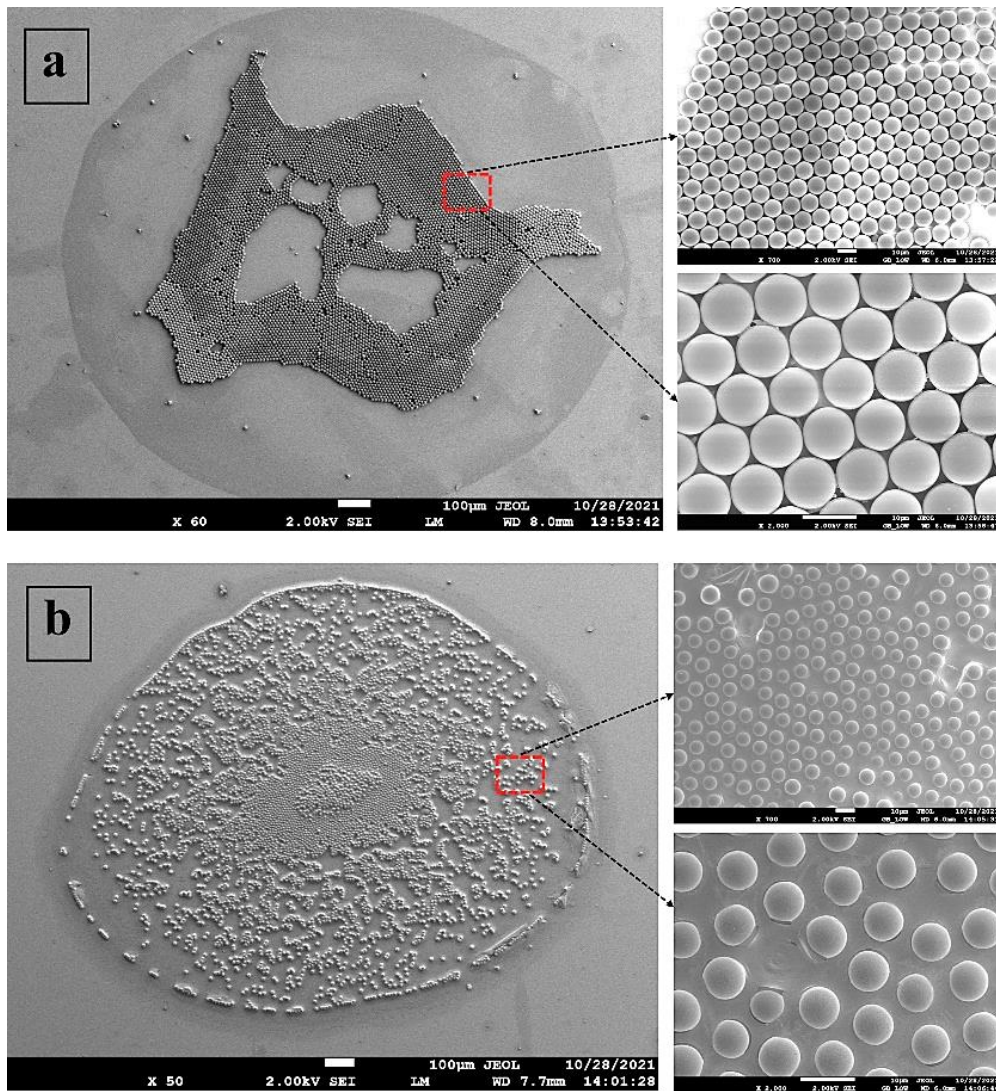


Figure 14: Scanning Electron Microscopy images of dried droplet patterns of 10-micron sized particles (a) In DI water (b) In presence of salt.

It must be noted that in some of the dried patterns, formation of crystals/dendrites were observed. Studies report that the formation of crystals starts when the ionic concentration achieves the critical supersaturation concentration [22]. Thus, in the present case, when the deposited ions reached the supersaturation concentration, formation of crystals/dendrites were observed at the edge of the droplet. Also, the appearance of crystals/ dendrites depends on factors such as size and concentration of particles along with the type and concentration of salts [40]. It has been reported in the literature, that mono basic salts lead to formation of grid like patterns, di-basic salts appear to have branched structures and tri-basic salts form no

patterns [40], which are in line with the current observations. It must be re-iterated that the aim of the current work was to explore the sole effect of salts on the final dried patterns of model solutions, due to its presence in body fluids and buffer solutions (as mentioned previously). The detailed kinetics of crystal/dendritic growth and how the presence of polystyrene particles can alter the formation of these crystals/ dendrites would be a part of the future work.

5. Conclusion:

In the current investigation, the sole influence of six commonly available salts with multivalent co-ions viz. NaCl, Na₂HPO₄, NaH₂PO₄, Na₂SO₄, MgSO₄ and Na₃PO₄ on the final dried patterns of model solutions have been explored to better understand the underlying mechanisms involved during the drying of complex fluids. Polystyrene particles (of sizes 1 μm, 3 μm, 7 μm and 10 μm) and salts were mixed in different volumetric ratios to prepare the model solutions. The inclusion of salts induced an additional inward flow from the edge of the droplet to the center, thus carrying the particles away from the contact line and suppressing the formation of coffee ring, in particles of sizes 1 and 3 microns. On the other hand, the combined effect of the higher settling velocities (in particles of sizes 7 and 10 microns) along with the inward base flow, resulted in the formation of central clusters for the bigger particles, in presence of salts. The findings of the current objective can provide an initial understanding of the effect of multivalent co-ions on the overall drying deposition patterns of complex fluids to further aid in detection of diseases.

References:

- [1] R. D. Deegan, O. Bakajin, T. F. Dupont, G. Huber, S. R. Nagel, and T. A. Witten, *Capillary Flow as the Cause of Ring Stains from Dried Liquid Drops*, Nature 1997 389:6653 **389**, 827 (1997).
- [2] M. Parsa, S. Harmand, and K. Sefiane, *Mechanisms of Pattern Formation from Dried Sessile Drops*, Advances in Colloid and Interface Science.
- [3] K. Sefiane, *Patterns from Drying Drops*, Adv Colloid Interface Sci **206**, 372 (2014).
- [4] S. G. Subramanian, S. Nair, and S. DasGupta, *Evaporation Mediated Translation and Encapsulation of an Aqueous Droplet atop a Viscoelastic Liquid Film*, J Colloid Interface Sci **581**, 334 (2021).

- [5] R. Bhardwaj, X. Fang, P. Somasundaran, and D. Attinger, *Self-Assembly of Colloidal Particles from Evaporating Droplets: Role of DLVO Interactions and Proposition of a Phase Diagram*, *Langmuir* **26**, 7833 (2010).
- [6] J. R. Moffat, K. Sefiane, and M. E. R. Shanahan, *Effect of TiO₂ Nanoparticles on Contact Line Stick-Slip Behavior of Volatile Drops*, *Journal of Physical Chemistry B* **113**, 8860 (2009).
- [7] B. Mook Weon and J. Ho Je, *Fingering inside the Coffee Ring*, *Phys Rev E* **87**, 13003 (2013).
- [8] X. Zhong, J. Ren, and F. Duan, *Wettability Effect on Evaporation Dynamics and Crystalline Patterns of Sessile Saline Droplets*, *Journal of Physical Chemistry B* **121**, 7924 (2017).
- [9] D. Mampallil and H. B. Eral, *A Review on Suppression and Utilization of the Coffee-Ring Effect*, *Adv Colloid Interface Sci* **252**, 38 (2018).
- [10] U. U. Ghosh, G. Subramanian, S. Chakraborty, and S. Dasgupta, *Droplets in Microfluidics*, (n.d.).
- [11] R. Chen, L. Zhang, D. Zang, and W. Shen, *Blood Drop Patterns: Formation and Applications*, *Adv Colloid Interface Sci* **231**, 1 (2016).
- [12] M. Mukhopadhyay, U. U. Ghosh, D. Sarkar, and S. Dasgupta, *Surface Property Induced Morphological Alterations of Human Erythrocytes*, *Soft Matter* **14**, 7335 (2018).
- [13] M. Mukhopadhyay, R. Ray, M. Ayushman, P. Sood, M. Bhattacharyya, D. Sarkar, and S. DasGupta, *Interfacial Energy Driven Distinctive Pattern Formation during the Drying of Blood Droplets*, *J Colloid Interface Sci* **573**, 307 (2020).
- [14] M. Mukhopadhyay, S. G. Subramanian, K. V. Durga, D. Sarkar, and S. DasGupta, *Laser Printing Based Colorimetric Paper Sensors for Glucose and Ketone Detection: Design, Fabrication, and Theoretical Analysis*, *Sens Actuators B Chem* **371**, 132599 (2022).
- [15] A. Pal, A. Gope, A. S. Athair, and G. S. Iannacchione, *A Comparative Study of the Drying Evolution and Dried Morphology of Two Globular Proteins in De-Ionized Water Solutions*, *RSC Adv* **10**, 16906 (2020).
- [16] A. Sett, M. Ayushman, S. Desgupta, and S. Dasgupta, *Analysis of the Distinct Pattern Formation of Globular Proteins in the Presence of Micro- and Nanoparticles*, *Journal of Physical Chemistry B* **122**, 8972 (2018).
- [17] B. Pathak, J. Christy, K. Sefiane, and D. Gozuacik, *Complex Pattern Formation in Solutions of Protein and Mixed Salts Using Dehydrating Sessile Droplets*, *Langmuir* **36**, 9728 (2020).
- [18] Y. J. P. Carreón, M. Ríos-Ramírez, P. Vázquez-Vergara, S. Salinas-Almaguer, I. Cipriano-Urbano, A. Briones-Aranda, O. Díaz-Hernández, G. J. Escalera Santos, and J. González-Gutiérrez, *Effects of Substrate Temperature on Patterns Produced by Dried Droplets of Proteins*, *Colloids Surf B Biointerfaces* **203**, (2021).
- [19] M. Efstratiou, J. Christy, D. Bonn, and K. Sefiane, *The Effect of Substrate Temperature on the Evaporative Behaviour and Desiccation Patterns of Foetal Bovine Serum Drops*, *Colloids and Interfaces* **5**, 43 (2021).
- [20] M. Efstratiou, J. Christy, and K. Sefiane, *Crystallization-Driven Flows within Evaporating Aqueous Saline Droplets*, *Langmuir* **36**, 4995 (2020).
- [21] V. Soulié, S. Karpitschka, F. Lequien, P. Prené, T. Zemb, H. Mochwald, and H. Riegler, *The Evaporation Behavior of Sessile Droplets from Aqueous Saline Solutions*, *Physical Chemistry Chemical Physics* **17**, 22296 (2015).

- [22] X. Shao, Y. Hou, and X. Zhong, *Modulation of Evaporation-Affected Crystal Motion in a Drying Droplet by Saline and Surfactant Concentrations*, Colloids Surf A Physicochem Eng Asp **623**, (2021).
- [23] N. Shahidzadeh, M. F. L. Schut, J. Desarnaud, M. Prat, and D. Bonn, *Salt Stains from Evaporating Droplets*, Sci Rep **5**, (2015).
- [24] G. Xu, W. Hong, W. Sun, T. Wang, and Z. Tong, *Effect of Salt Concentration on the Motion of Particles near the Substrate in Drying Sessile Colloidal Droplets*, Langmuir **33**, 685 (2017).
- [25] D. O. Kim, M. Pack, H. Hu, H. Kim, and Y. Sun, *Deposition of Colloidal Drops Containing Ellipsoidal Particles: Competition between Capillary and Hydrodynamic Forces*, Langmuir **32**, 11899 (2016).
- [26] V. R. Dugyala and M. G. Basavaraj, *Control over Coffee-Ring Formation in Evaporating Liquid Drops Containing Ellipsoids*, Langmuir **30**, 8680 (2014).
- [27] S. Devineau, M. Anyfantakis, L. Marichal, L. Kiger, M. Morel, S. Rudiuk, and D. Baigl, *Protein Adsorption and Reorganization on Nanoparticles Probed by the Coffee-Ring Effect: Application to Single Point Mutation Detection*, J Am Chem Soc **138**, 11623 (2016).
- [28] J. Y. Jung, Y. W. Kim, J. Y. Yoo, J. Koo, and Y. T. Kang, *Forces Acting on a Single Particle in an Evaporating Sessile Droplet on a Hydrophilic Surface*, Anal Chem **82**, 784 (2010).
- [29] T. S. Wong, T. H. Chen, X. Shen, and C. M. Ho, *Nanochromatography Driven by the Coffee Ring Effect*, Anal Chem **83**, 1871 (2011).
- [30] H. Hu and R. G. Larson, *Analysis of the Effects of Marangoni Stresses on the Microflow in an Evaporating Sessile Droplet*, Langmuir **21**, 3972 (2005).
- [31] Jacob N. Israelachvili, *Intermolecular and Surface Forces*, Vol. Third edition (2011).
- [32] R. Iqbal, B. Majhy, A. Q. Shen, and A. K. Sen, *Evaporation and Morphological Patterns of Bi-Dispersed Colloidal Droplets on Hydrophilic and Hydrophobic Surfaces*, Soft Matter **14**, 9901 (2018).
- [33] N. D. Patil, R. Bhardwaj, and A. Sharma, *Self-Sorting of Bidispersed Colloidal Particles Near Contact Line of an Evaporating Sessile Droplet*, Langmuir **34**, 12058 (2018).
- [34] V. H. Chhasatia and Y. Sun, *Interaction of Bi-Dispersed Particles with Contact Line in an Evaporating Colloidal Drop*, Soft Matter **7**, 10135 (2011).
- [35] L. K. Malla, R. Bhardwaj, and A. Neild, *Analysis of Profile and Morphology of Colloidal Deposits Obtained from Evaporating Sessile Droplets*, Colloids Surf A Physicochem Eng Asp **567**, 150 (2019).
- [36] H. Hu and R. G. Larson, *Analysis of the Microfluid Flow in an Evaporating Sessile Droplet*, Langmuir **21**, 3963 (2005).
- [37] G. Upadhyay and R. Bhardwaj, *Colloidal Deposits via Capillary Bridge Evaporation and Particle Sorting Thereof*, Langmuir **37**, 12071 (2021).
- [38] Y. S. Yu, M. C. Wang, and X. Huang, *Evaporative Deposition of Polystyrene Microparticles on PDMS Surface*, Sci Rep **7**, (2017).
- [39] A. S. Sangani, C. Lu, K. Su, and J. A. Schwarz, *Capillary Force on Particles near a Drop Edge Resting on a Substrate and a Criterion for Contact Line Pinning*, Phys Rev E Stat Nonlin Soft Matter Phys **80**, (2009).

- [40] S. Paria, R. Ghosh Chaudhuri, and N. N. Jason, *Self-Assembly of Colloidal Sulfur Particles on a Glass Surface from Evaporating Sessile Drops: Influence of Different Salts*, *New Journal of Chemistry* **38**, 5943 (2014).

